RSC Advances

PAPER

View Article Online
View Journal | View Issue

Cite this: *RSC Adv.*, 2023, **13**, 3193

$La_2CoO_{4+\delta}$ perovskite-mediated peroxymonosulfate activation for the efficient degradation of bisphenol A

Xin Zhong, *[ab] Wenting Wu,[b] Haonan Jie[b] and Fubin Jiang[a]

Sulfate radical-based technology has been considered as an efficient technology to remove pharmaceuticals and personal care products (PPCPs) with heterogeneous metal-mediated catalysts for the activation of peroxymonosulfate (PMS). In this study, $La_2CoO_{4+\delta}$ perovskite with Ruddlesden–Popper type structure was synthesised by the sol–gel method, which was employed in PMS activation. Different characteriazation technologies were applied for the characterization of $La_2CoO_{4+\delta}$, such as SEM-EDX, XRD, and XPS technologies. A common organic compound, bisphenol A (BPA), is used as a target contaminant, and the effect impactors were fully investigated and explained. The results showed that when the dosage of $La_2CoO_{4+\delta}$ was 0.5 g L^{-1} and the concentration of PMS was 1.0 mM in neutral pH solution, about 91.1% degradation efficiency was achieved within 25 minutes. Quenching experiments were introduced in the system to verify the catalytic mechanism of PMS for the BPA degradation, proving the existence of superoxide, hydroxyl radicals and sulfate radicals, which are responsible for the catalytic degradation of BPA. Moreover, the reusability and stability of the catalyst were also conducted which showed good stability during the reaction. This work would improve the applications of A_2BO_4-type perovskites for activating PMS to degrade BPA.

Received 1st December 2022
Accepted 14th January 2023

DOI: 10.1039/d2ra07640c

rsc.li/rsc-advances

1. Introduction

In recent decades, the increasing water contamination problem has received more attention, and is caused mostly by recalcitrant organic compounds.[1–4] These compounds usually leave trace concentrations in the effluent, which degrade slowly in the environment and are also difficult to remove by the conventional processes, such as the activated sludge method, coagulation and flocculation, precipitation and absorption.[5–7] Bisphenol A is widely used as a synthetic material in various areas not only in the production of water bottles but also for livestock.[8] It is reported that the trace concentration of BPA compounds has been reported to be detected in water, soil and sewage.[9–11] The residual BPA in the environment can cause side effects in humans, resulting in endocrine disorders, obesity and even cancer.[12] It is crucial to explore efficient and environmentally friendly methods for the degradation of BPA in the environment to minimize the side effects of the residuals.

Advanced oxidation processes (AOPs) have been widely used to degrade the recalcitrant organic pollutants in water.[13–16] The role of AOPs is to combine homogeneous/heterogeneous metal-mediated catalysts with certain oxidants (such as H_2O_2, peroxymonosulfate/persulfate and/or oxygen) in order to generate the reactive oxidant species for the mineralization of organic pollutants with low toxicity or even harmlessness to the environment.[17–19] Hydroxyl radicals are the commonly used radicals in AOPs, which have high removal efficiency to degrade the pollutants but suffer acidic reaction conditions, short half-life time and non-selective to the pollutants.[20–22] To overcome this shortage, the sulfate radical-based technology (SR-AOP) has been going through full development, due to its higher oxidative potential, longer half-life time and milder reaction conditions with a wide range of pH solutions.[23–25] Peroxymonosulfate (PMS) is often used as an oxidant in SR-AOP in order to produce the sulfate radicals, which can be activated by many methods. In contrast to the energy-based activation, such as solar/UV, ultrasound, electrical and thermal activation, the catalytic activation is more commonly used due to its low-cost and efficiency in the decomposition of PMS by transition metal ions and heterogeneous catalysts.[26–28] In the SR-AOP systems, many reactive oxygen species, including hydroxyl radicals, singlet oxygen and superoxide, can be generated in the presence of heterogeneous perovskite catalysts, such as $La_2CuO_{4+\delta}$,[29] $LaFe_{1-x}Co_xO_3$,[30] $LaCoO_3$ [31] and $LaRuO_3$.[32] Moreover, the system of heterogeneous catalyst activated PMS has received more attention, since the separation of heterogeneous catalysts is more feasible and prevent the secondary pollution problem in the homogenous systems. Thanks to the presence of reactive oxidant species, the activation efficiency is excellent, the reaction operation is less complex, the cost is lower (compared with

[a]*Experimental and Practical Innovation Education Centre, Beijing Normal University at Zhuhai, Zhuhai, China. E-mail: zhongxin@bnu.edu.cn; Tel: +86-756-3621560*
[b]*College of Real Estate, Beijing Normal University, Zhuhai, Zhuhai, China*

the energy-based sulfate radical processes) and the metal ions leached in the water effluent was limited in the heterogeneous systems.

The perovskite catalyst possessed the ABO_3 structure, in which A and B are often used as earth metals and transition metals.[33–35] Many elements are chosen to form the perovskite structure, and even the substitution of partial elements would still maintain the structure without detriment.[36] Among various transition metal ions, cobalt-based perovskites attract more attention and show good catalytic efficiency and stability with limited cobalt ions leaching in the reaction.[37] The redox active Co(III)/Co(II) pairs facilitate the feasible transition on the catalyst surface. To boost the catalytic efficiency, many efforts have been made.[38–40] First, a smaller particle size and larger pore diameter with a higher BET surface area could provide more active sites for the subsequent reaction. On the other hand, the A-site and B-site would be partially substituted by other ions with cation deficient to regulate the surface physicochemical properties, which exhibit inspiring catalytic performance due to the generation of oxygen vacancies. However, compared with ABO_3-type perovskites, A_2BO_4-type perovskites could exhibit more feasibility in the redox pair transition and show good stability due to their structure for more extra spaces between A-site and B-site atoms.[41] This kind of perovskite consists of ABO_3 and rock salt (AO) layers, which along with the Ruddlesden–Popper mixed oxides (R–P type), exhibiting better exchange and oxygen diffusion than other types of perovskites. Several studies on the R–P-type perovskites were used for the activation of PMS for the degradation of chemical pollutants.[42–44] To the best of our knowledge, there are few studies on the activation of PMS by $La_2CoO_{4+\delta}$ for the degradation of BPA.

Based on the above results, in this study, perovskite $La_2CoO_{4+\delta}$ (LCO) with was fabricated *via* sol–gel methods and used as a catalytic activator for PMS to remove BPA from water. The physicochemical properties and morphology of LCO have been systematically characterized by many techniques. In addition, the effect of different experimental conditions on the BPA degradation efficiency and different water matrices, including pure water, Xijiang river water (XW) and sea water (SW), was tested. Further experiments were carried out, such as the reusability, kinetics and mechanism in the system, in order to evaluate the actual application potential of LCO. Additionally, the quenching experiments were conducted to investigate the degradation mechanism. The goal of the study was to obtain the LCO with a very low amount of cobalt leaching into the water to obtain the environmental requirements. This research offered a creative idea about the high catalytic activity of LCO in the decomposition of PMS, which provides a new way to illustrate the mechanism of the LCO/PMS process in actual wastewater.

2. Materials and methods

2.1. Chemicals

The chemical reagents were all analytical grade and used without further purification. For the synthesis of the perovskites, lanthanum nitrate hexahydrate ($La(NO_3)_3\cdot 6H_2O$), cobalt nitrate ($Co(NO_3)_2\cdot 6H_2O$), and oxone ($KHSO_5\cdot 0.5KHSO_4\cdot 0.5K_2SO_4$) were purchased from Rhawn Industrial Corporation (China). The other chemical reagents were purchased from Aladdin Industrial Corporation. Solutions were prepared by in deionized water.

2.2. Preparation and characterization of LCO

The sol–gel method was employed to synthesize the LCO particles. Amounts of $La(NO_3)_3\cdot 6H_2O$, citric acid and $Co(NO_3)_2\cdot 6H_2O$ were appropriately weighed (with molar ratio of 2 : 3 : 1, 2.98 g, 1.98 g and 1.0 g, respectively) and dissolved in 15 mL of deionized water under vigorous stirring at room temperature. The obtained homogeneous mixture was stirred in water bath for 2 h at 80 °C to make water evaporated slowly and the wet pink-peach gel was obtained which is sticky to flow. The substance was dried at 120 °C for 12 h in air to ensure that substance was completely dried. The dried powder was calcined in muffle furnace in air with the heating rate of 2 °C min^{-1} up to 550 °C and temperature remains for 4 h, and the desired perovskite LCO catalyst was got.

X-ray diffraction (XRD) patterns were obtained using a Bruker D8ADVANCE X-ray diffractometer with a graphite monochromatic Cu Kα radiation ($\lambda = 1.54$ Å) at an accelerating voltage of 40 kV and a current of 30 mA over a 2θ scanning range of 10°–80°. Scanning electron microscopy (SEM) was performed on a Hitach SU8220 field emission with an X-ray energy dispersive spectra (EDS) instrument to determine the element distribution. The X-ray photoelectron spectroscopy (XPS) was conducted to obtain the surface chemical information with a Thermo Fisher ESCALAB250Xi. The textural properties of the samples were analysed by N_2 adsorption–desorption technology using automatic Micromeritics Instrument Corporation TriStar II 3020.

2.3. Experimental procedures

In this study, a certain amount of PMS was added to a 250 mL glass beaker containing 100 mL BPA solution at 0.05 mM. The pH solution was maintained unadjusted, which was a neutral pH of 6.8 ± 0.2. The reaction was performed at room temperature (25 ± 2 °C) with magnetic stirring at 500 rpm. At first, 0.5 g L^{-1} catalyst was added to the BPA solution in advance. At certain time intervals, 1 mL samples were collected by syringe and filtered through 0.22 μm membranes to remove the catalyst, and then the sample was mixed with 10 μL methanol (MeOH) to terminate the reaction before analysis by high-performance liquid chromatography (HPLC). The concentration of BPA was measured *via* a high-pressure liquid chromatography (HPLC) system (LC-16, Shimadzu) which was equipped with a C18 (4.6 mm × 150 mm, 5 mm) column and a UV detector which set at 278 nm. The mobile phase was 70% MeOH and 30% ultrapure water, and the speed was set to 1.0 mL min^{-1}. Experiments were conducted at least three times, and the average value was used.

In the typical quenching experiments, methanol (MeOH) was employed to capture hydroxyl radicals and sulfate radicals. *Tert*-butyl alcohol (TBA) was used for scavenging hydroxyl radicals. Benzoquinone (BQ) was used to scavenge superoxide radicals.

Moreover, in the reusability experiments, the catalyst was centrifuged at 8000 rpm for 7 min. The obtained catalyst was washed with deionized water in order to remove the residual chemicals on the surface of the catalyst, and then re-dispersed into fresh BPA solution for the next experiment run.

3. Results and discussion

3.1. Physicochemical characteristics of LCO

As shown in Fig. 1, the X-ray diffraction patterns of the LCO catalyst were consistent with previous reports, which exhibit a well crystallized perovskite phase. The characteristic diffraction peaks of the sample centred at 24.1°, 31.4°, 32.6°, 42.7° and 46.7° correspond to the representative reflections of the (111), (113), (200), (115) and (220) lattice planes, respectively. The average crystalline size was calculated to be approximately 14 nm according to the Scherrer equation.[20] Nearly no impurity peaks or deviations were observed in the patterns. The $La_2CoO_{4+\delta}$ diffraction peaks show a good match to a Ruddlesden–Popper type phase of La_2CoO_4 (No. 72-0937).[44] The sharp phase of LCO pointed out indicated the good crystallinity and small crystal size of the as-synthesized catalyst. The XRD patterns were maintained during the LCO/PMS process, indicating the stability of the LCO catalyst. In addition, the adsorption isotherms of the LCO catalyst were also investigated with a type IV isotherm, which evidenced the presence of a mesoporous structure. The BET surface area of the samples was 6.85 $m^2\ g^{-1}$ with a pore diameter of 23.1 nm which confirmed the mesoporous structure of LCO.

The morphology of the LCO catalyst was determined by SEM, as shown in Fig. 2. The catalyst was observed in consists of smooth irregular agglomerates with clear boundaries. As measured by EDX, the catalyst sample is composed of three elements, La, Co and O, where the average atomic percentage of La and Co was calculated as 2.23 (the La/Co atomic ratio) and the La/O atomic ratio was 2.41. This atomic ratio was really close to the standard stoichiometric ratio, indicating that the catalyst was successfully synthesized. The mapping images of the LCO catalyst were also observed and are shown in Fig. 2(d)–(f). The results showed that three elements, La, Co and O, was participated in the catalyst all over the surface. The distribution of Co species on the surface of the catalyst could be a good activator in the activation of PMS, leading to the generation of reactive species for the elimination of BPA.

In order to explore the surface properties of the LCO catalyst, XPS measurements were carried out.[45] As shown in Fig. 3, the survey spectra indicated that there are three elements present in the LCO catalyst. The double peaks centred at 850.6 eV and 854.9 eV were responsible for the La $3d_{3/2}$, and the double peaks centred at 833.7 eV and 837.4 eV were responsible for the La $3d_{5/2}$. Meanwhile, the peaks at 779.5 eV and 789.3 eV were corresponded to Co $2p_{3/2}$, and the peak at 781.4 eV was corresponded to Co $2p_{1/2}$, respectively. The high resolution of the O 1s XPS spectra is also observed in Fig. 3d. The O 1s peak could be

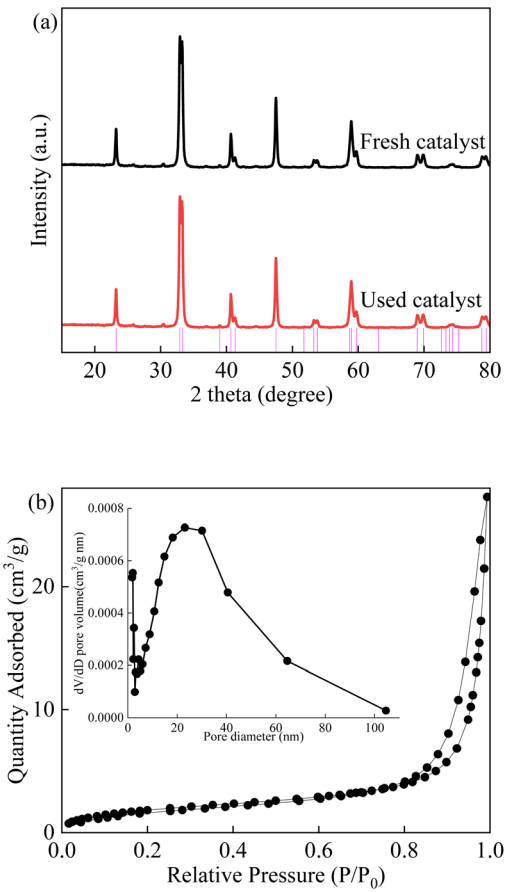

Fig. 1 (a) XRD patterns of fresh and used LCO catalyst; (b) isotherm image of LCO catalyst.

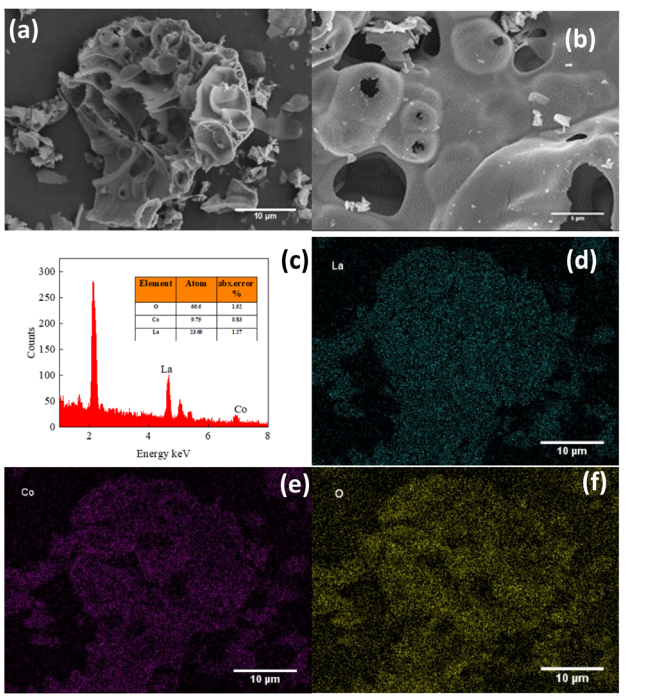

Fig. 2 (a and b) SEM images of LCO catalyst; (c) EDX spectra of LCO catalyst; (d–f) mapping images of LCO catalyst.

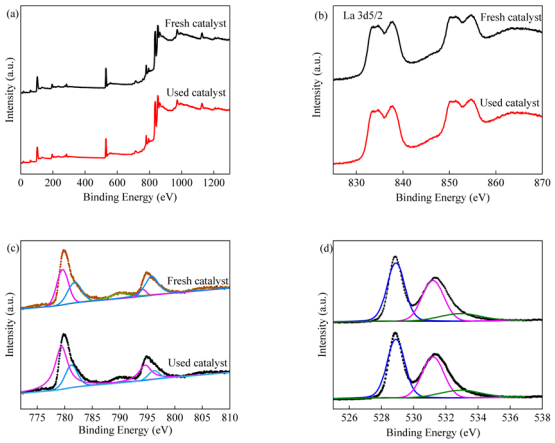

Fig. 3 XPS spectra of LCO (a) survey spectra; (b) La 3d; (c) Co 2p; (d) O 1s.

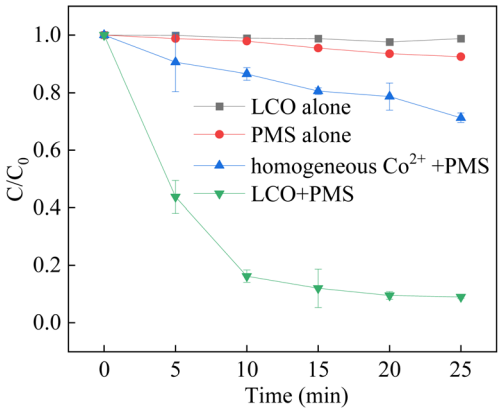

Fig. 5 BPA degradation in different reaction systems. Reaction conditions: [BPA] = 0.05 mM, [PMS] = 1.0 mM, [LCO] = 0.5 g L^{-1}, initial PH = 6.8.

deconvoluted into three single peaks at 528.8, 531.2 and 532.9 eV, indicating the presence of O^{2-}, the adsorbed oxygen species and the vibration stretching of hydroxyl groups of absorbed H_2O.[46–48]

As shown in Fig. 4, the two peaks near 400 cm^{-1} and 600 cm^{-1} were observed, which were attributed to the stretching and bending vibrations of the Co–O bond. The bands centred at 1390 cm^{-1} and 3500 cm^{-1} was corresponded to the residual nitrate and the H_2O molecules.[49]

3.2. Catalytic activity of catalyst

The degradation of BPA was investigated in different systems to verify the catalytic activity for the activation of PMS which shown in Fig. 5. The results showed that negligible BPA removal was observed by LCO alone, evidencing that the adsorption of the catalyst is limited. Meanwhile, it is observed that only 8.2% of BPA was observed by using PMS alone, which was attributed to little decomposition of PMS. With the presence of LCO and PMS, the removal efficiency was significant and reached to 91.1% in 25 min. However, the removal efficiency was only 28.8% in the presence of leaching concentrations of Co^{2+} (approximately 0.026 mg L^{-1}, measured by ICP-MS) and PMS. The results showed that the LCO played a major role in the activation of PMS. In order to evaluate the reaction kinetics of BPA elimination in the LCO/PMS process, a pseudo-first-order equation was expressed in eqn (1).

$$\ln(C_0/C_t) = K_{obs} \times t \quad (1)$$

where C_0 is the BPA concentration at 0.05 M, C_t is the BPA concentration during in the degradation process, K_{obs} represents the pseudo-first-order constant (min^{-1}) and t is the reaction time. The reaction constant of LCO/PMS was approximately 0.1175 min^{-1}, which was in good agreement with previous studies.[50–52] The results showed that the LCO exhibited high activity in the activation of PMS with the advantage of a short reaction time. The LCO catalyst could effectively activate PMS to generate reactive oxidant species for the rapid removal speed of BPA.

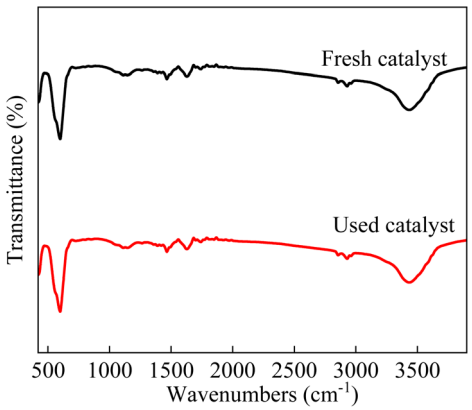

Fig. 4 FTIR spectra of fresh and used LCO catalyst.

3.3. Effect of catalyst dosage

To determine the effect of catalyst dosage on the removal of BPA, a series of different catalyst dosages were performed, as the catalyst was recognized as the provider of active sites for the decomposition of PMS.

As shown in Fig. 6, the degradation efficiency was accelerated by increasing the catalyst dosage from 0.1 g L^{-1} to 1.0 g L^{-1}. In addition, the reaction rate constant was also boosted from 0.0553 min^{-1} to 0.1294 min^{-1}. The results could be attributed to the occurrence of more active sites for the activation of PMS provided by the LCO catalyst.[53] Due to the presence of more active sites for the decomposition of PMS, more reactive oxidant species were generated, leading to higher degradation efficiency. However, when the catalyst dosage reached to 1.0 g L^{-1}, the increment of degradation efficiency and rate was not significant, as the rate constant reached to 0.1294 min^{-1}. It is speculated that the reason is the agglomeration effect of excess catalyst and the quenching experiment of radicals with each other. As a result, 0.5 g L^{-1} LCO catalyst was used for the subsequent experiments due to the economic concerns.

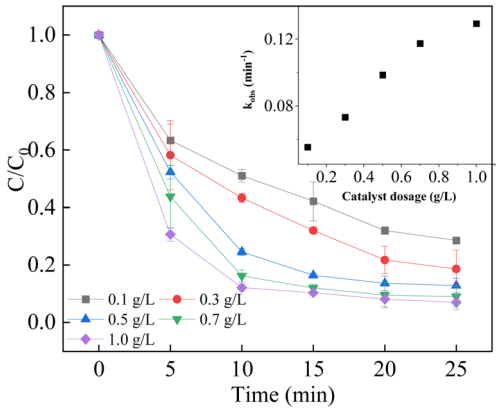

Fig. 6 Effect of catalyst dosage on BPA degradation. Reaction conditions: [BPA] = 0.05 mM, [PMS] = 1.0 mM, [LCO] = 0.1–1.0 g L^{-1}, initial PH = 6.8.

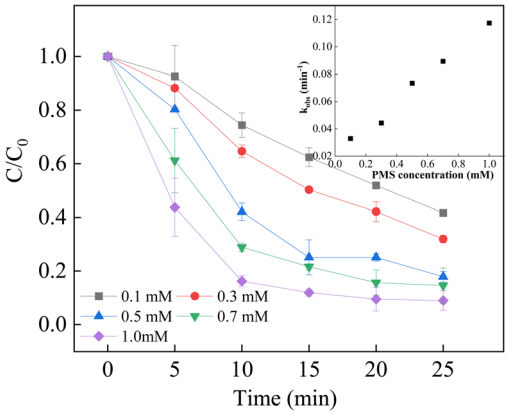

Fig. 7 Effect of PMS concentration on BPA degradation. Reaction conditions: [BPA] = 0.05 mM, [PMS] = 0.1–1.0 mM, [LCO] = 0.5 g L^{-1}, initial PH = 6.8.

$$^{\cdot}OH + {}^{\cdot}OH \rightarrow H_2O_2 \quad (2)$$

$$SO_4^{\cdot -} + SO_4^{\cdot -} \rightarrow S_2O_8^{2-} \quad (3)$$

$$SO_4^{\cdot -} + {}^{\cdot}OH \rightarrow HSO_5^{-} \quad (4)$$

3.4. Effect of PMS concentration

It has been reported that the PMS concentration efficiently affect the degradation efficiency and rate.[54–56] Used as the oxidant in the process, low PMS concentration in the system resulted in a weaken degradation efficiency due to less formation of reactive species, which was observed to result in a higher degradation efficiency with a higher PMS concentration. However, the high concentration of PMS might lead to the scavenging of excess PMS and sulfate radicals, causing a decrease in degradation efficiency. In this study, the degradation efficiency of BPA increased in good agreement with the increase in PMS concentration ranging from 0.1 mM to 1.0 mM, while the rate constant gradually increased from 0.033 min^{-1} to 0.1175 min^{-1}. When 1.0 mM PMS was used in the system, the rate constant was 0.1175 min^{-1}, which was slightly increased despite of the highest removal efficiency of BPA, which could be attributed to the scavenging effect. Based on these results, a 1.0 mM PMS concentration was selected as the optimal oxidant concentration for the subsequent experiments (Fig. 7).

3.5. Effect of pH

The pH solution affected the degradation removal of pollutants in the heterogenous catalyst/PMS system. The reaction slowed down with the increment of pH from 3.1 to 6.7, while the reaction slightly increased as the pH reached to 9.1. It can be concluded that the LCO catalyst would maintain activity over a wide pH range. Under acidic conditions, the catalyst surface could be positively charged, which facilitates the adsorption of HSO_5^- on the surface of the catalyst and the decomposition of PMS, leading to better degradation efficiency and rate. When the pH exceeded 9.1, the alkaline condition would lead to the formation of hydroxyl radicals as the reaction between sulfate radicals and OH-which observed with increment of degradation efficiency. With the increase of pH further up to >10.0, the surface of LCO was negatively charged. Moreover, partial PMS would be transferred to SO_5^-, which is considered more stable and hardly directly decomposed by the LCO catalyst, resulting in the decline of in the BPA degradation rate (Fig. 8).[57–59]

3.6. Effect of Co-existing ions and natural organic matter (NOM)

The presence of inorganic anions in natural water played a great major role in the degradation process of BPA. Fig. 9 shows that the influence of HCO_3^- and Cl^- was significant, where Cl^- exhibited a slight promoting impact and HCO_3^- was regarded as a radical scavenger.[60–62] As shown in Fig. 9a, the presence of Cl^- promoted the degradation process at low concentrations. The reaction between Cl^- and hydroxyl radicals, and sulfate radicals led to the formation of $^{\cdot}Cl$ and $^{\cdot}ClOH$. Although their redox potential was lower than the redox potential of sulfate radicals and hydroxyl radicals, they showed good attack ability

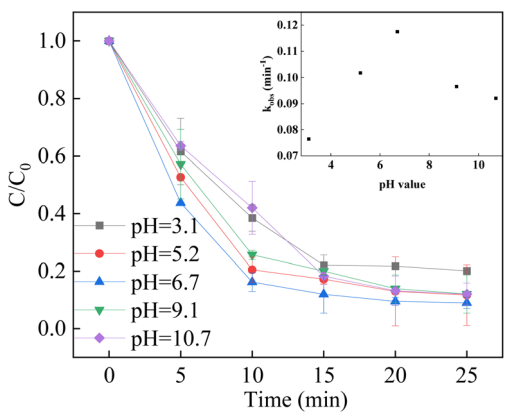

Fig. 8 Effect of initial pH on BPA degradation. Reaction conditions: [BPA] = 0.05 mM, [PMS] = 1.0 mM, [LCO] = 0.5 g L^{-1}, initial PH = 3.1–9.1.

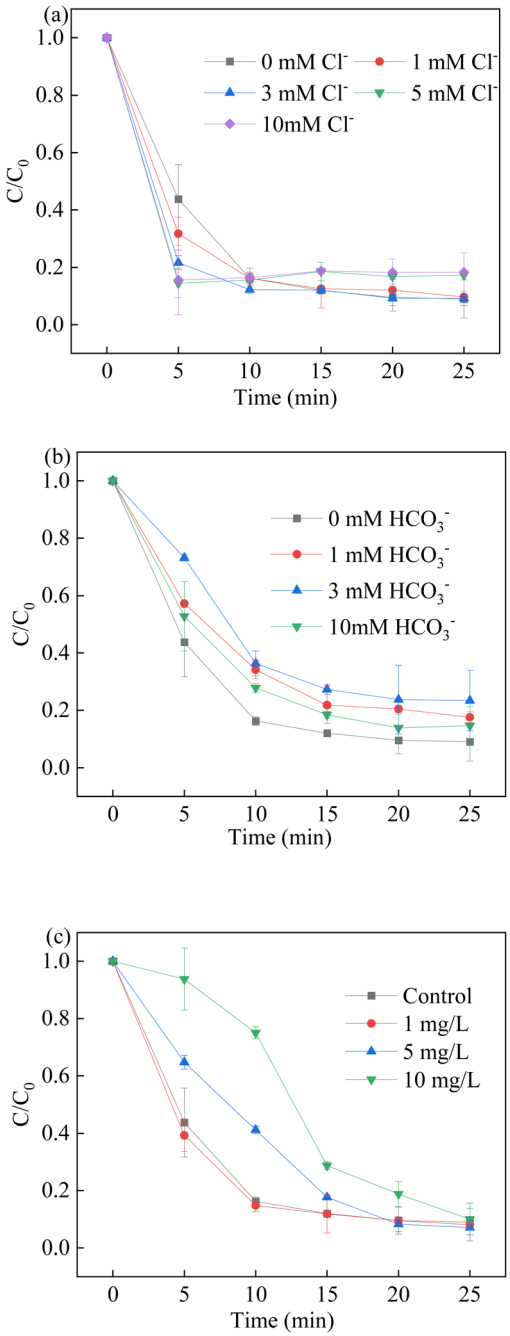

Fig. 9 Effect of co-existing ions (a) Cl^-; (b) HCO_3^- and (c) natural organic matter on BPA degradation. Reaction conditions: [BPA] = 0.05 mM, [PMS] = 1.0 mM, [LCO] = 0.5 g L^{-1}, initial PH = 6.8.

against BPA with a high-rate constant. As a result, a higher BPA degradation rate was observed in the presence of Cl^-. However, the excess of Cl^- did not further promote BPA removal. The excess Cl^- would participate in the quenching experiments in which chlorine species of lower redox potential were generated. Moreover, the presence of 5 mM Cl^- led to an insignificant effect on the BPA removal.

$$Cl^- + HSO_5^- \rightarrow SO_4^{2-} + HClO \quad (5)$$

$$Cl^- + SO_4^{\cdot -} \rightarrow {}^{\cdot}Cl + SO_4^{2-} \quad (6)$$

$$Cl^- + {}^{\cdot}OH \rightarrow {}^{\cdot}ClOH \quad (7)$$

$${}^{\cdot}ClOH + H^+ \rightarrow {}^{\cdot}Cl + H_2O \quad (8)$$

$${}^{\cdot}Cl + Cl^- \rightarrow {}^{\cdot}Cl_2^- \quad (9)$$

It is reported that HCO_3^- could be able to react with hydroxyl radicals and sulfate radicals to produce $CO_3^{\cdot -}$ in the reaction, which is recognized as a radical scavenger for the elimination of free radicals. In contrast to sulfate radicals and hydroxyl radicals, the generation of $CO_3^{\cdot -}$ and $HCO_3^{\cdot -}$ had a negative effect on the BPA degradation, which suffered a low reaction rate with target pollutants. In addition, the pH of solution increased due to the presence of HCO_3^-, and the alkaline conditions had a positive effect on the BPA removal. The positive effect offset the negative effect; thus, the inhibition of BPA removal was similar at different concentrations of HCO_3^-.

$${}^{\cdot}OH + HCO_3^- \rightarrow CO_3^{\cdot -} + H_2O \quad (10)$$

$$SO_4^{\cdot -} + HCO_3^- \rightarrow CO_3^{\cdot -} + SO_4^{2-} + H^+ \quad (11)$$

The effect of natural organic matter (NOM) was used to investigate the potential practical application on LCO/PMS system. Humic acid (HA) was employed in the system. The removal efficiency and rate were inhibited with the presence of 1.0 mg L^{-1}, 5.0 mg L^{-1} and 10.0 mg L^{-1} HA. The results showed that the scavenging effect of NOM on the free radicals happened when the HA was 5 mg L^{-1} and 10 mg L^{-1}, such as sulfate radicals and hydroxyl radicals. When the HA concentration was 1.0 mg L^{-1}, the degradation efficiency was a little higher than the controlled runs. The results showed that the HA was available to activate PMS for the generation of free radicals, due to the formation of semiquinone radicals.[29] On the other hand, the coordination between HA and LCO could lead to the generation of hydroxyl radicals and super oxidant in the solution. Based on the above results, low concentration of HA would facilitate the BPA degradation in the LCO/PMS systems.[30] The removal rate of BPA was inhibited with the presence of 10.0 mg L^{-1}, which could be ascribed to the scavenging effect of NOM to the free radicals.

3.7. Quenching experiments

Methanol (MeOH) is usually regarded as a scavenger of both hydroxyl radicals (k = 1.2–1.8 × 10^9 M^{-1} s^{-1}) and sulfate radicals (k = 1.6–7.8 × 10^7 M^{-1} s^{-1}), and *tert*-butanol (TBA) is a reactive scrubber for hydroxyl radicals (4–9 × 10^5 M^{-1} s^{-1}).[63–65] It is observed that mild inhibition was observed to be obtained within the presence of 50 mM of MeOH and TBA. However, when the 200 mM MeOH and TBA were introduced to the system, the removal efficiency was significantly decreased. The results showed that the sulfate radicals and hydroxyl radicals played a major role in the degradation of BPA. In addition, superoxide was also found in the heterogeneous activation of

PMS.[66–68] It is necessary to prove the existence of superoxide in the LCO/PMS. Thus, BQ was used as a scrubber for the superoxide (2.9×10^9 M^{-1} s^{-1}). It is observed that the addition of BQ efficiently suppressed the BPA removal efficiency, indicating that $O_2^{\bullet-}$ also participated in the degradation of BPA in the LCO/PMS systems. The results could be ascribed to the scavenging effect of hydroxyl radicals to BQ, as the rate constant of hydroxyl radicals was 1.2×10^9 M^{-1} s^{-1}. However, the superoxide suffered shorter half-life (1 ns) than that of sulfate radicals (30–40 μs) and hydroxyl radicals (20 ns). As a result, both $^{\bullet}OH$ and $SO_4^{\bullet-}$ are the major reactive species contributing to the BPA degradation (Fig. 10).

As can be seen in the XPS spectra, the La^{3+} valence in LCO was unchanged before and after the reaction, indicating that the perovskite structure was maintained during the catalytic reaction. The high-resolution XPS spectra of Co showed that the proportions of Co(II)/Co(III) were lower after the catalytic reaction, suggesting the participation of Co species in the reaction with the electron transfer between low valence and high valence. The intensity of the O 1s region was slightly increased after the reaction, as the high-resolution peaks could be deconvoluted into three constituents. The proportion of hydroxyl groups increased slightly after the reaction, while the adsorbed oxygen species decreased, indicating that the consumption of adsorbed oxygen species would lead to the formation of superoxide species.[69] The combination of reactive oxidant species would facilitate the degradation of BPA. Based on the above studies, a proposed reaction mechanism was given and illustrated. At first, the consumption of PMS occurred on the surface of the LCO catalyst with Co species, leading to the formation of sulfate radicals and hydroxyl radicals. Co(II) can be oxidized to Co(III) by the presence of HSO_5^-, while the reverse reduction reaction occurred by the transfer of Co(III) to Co(II) with the generation of SO_5^-. Based on the quenching experiments, except for the major role of sulfate radicals and hydroxyl radicals, superoxide also participate in the LCO/PMS systems for the degradation of BPA. Oxygen vacancies could facilitate the adsorption of PMS on the surface of catalyst due to the defects and the interfacial electron transfer for the generation of reactive oxidant species. On the other hand, the oxygen vacancies would also affect the chemical state and value of cobalt species, promoting the catalytic activity.[29] Through the reaction between HSO_5^- absorbed on LCO and oxygen vacancies, the $O_o^{\times}$ was formed and participated in the reaction which represents the oxygen ions in a normal oxygen site. During the generation of $O_o^{\times}$, the singlet oxygen was formed. Unfortunately, the singlet oxygen was not detected in this study. Additionally, the formation of singlet oxygen would arouse by the recombination of superoxide which consumed H^+. However, the main reaction was conducted in neutral pH value. It could be reasonable to speculate that the existence of superoxide in the solution which formed by a series of reactions.

$$\text{S–Co(II)} + HSO_5^- + \text{OVs} \rightarrow \text{S–Co(III)} + SO_4^{\bullet-} + OH^- + O_o^{\times} \quad (12)$$

$$\text{S–Co(III)} + HSO_5^- + O_o^{\times} \rightarrow \text{S–Co(II)} + SO_5^{\bullet-} + H^+ + \text{OVs} \quad (13)$$

$$SO_4^{\bullet-} + H_2O \rightarrow {}^{\bullet}OH + SO_4^{2-} + H^+ \quad (14)$$

$$SO_5^{\bullet-} + SO_5^{\bullet-} \rightarrow SO_4^{\bullet-} + SO_4^{\bullet-} + O_2 \quad (15)$$

$$\text{OVs} + HSO_5^- \rightarrow {}^1O_2 + SO_4^{2-} + H^+ \quad (16)$$

$$O_o^{\times} + HSO_5^- \rightarrow {}^1O_2 + HSO_4^- \quad (17)$$

$$O_2^{\bullet-} + 2H^+ \rightarrow 0.5{}^1O_2 + 0.5H_2O_2 \quad (18)$$

$$^{\bullet}OH + H_2O_2 \rightarrow H^+ + O_2^{\bullet-} + H_2O \quad (19)$$

$$OH^- + {}^{\bullet}OH + H_2O_2 \rightarrow O_2^{\bullet-} + 2H_2O \quad (20)$$

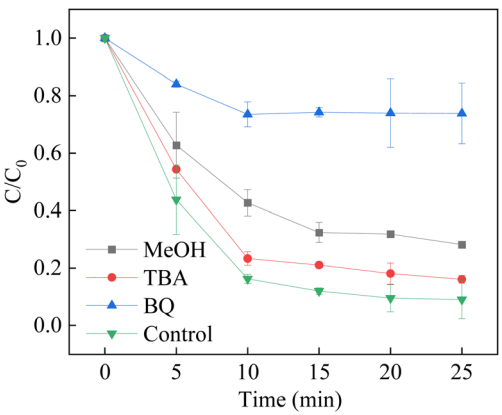

Fig. 10 Effect of radical scavengers on BPA degradation. Reaction conditions: [BPA] = 0.05 mM, [PMS] = 1.0 mM, [LCO] = 0.5 g L^{-1}, initial PH = 6.8, [scavengers] = 0.2 M.

3.8. Reusability and stability of the LCO catalyst

To evaluate the stability of the LCO catalyst, the LCO catalyst was collected and washed several times with deionized water for the reusability experiments. As shown in Fig. 11a, the degradation rate of BPA was observed a slight decrease, but the degradation efficiency remained constant during the first three runs. This result could be attributed to the partial loss of reactive sites during the reaction, which might be occupied by the intermediates or the inhibition of the reduction lattice oxygen. The removal performance of BPA in the last two runs was observed a decline, owing to the accumulation of intermediate by-products on the surface of reused LCO catalysts. The residual chemicals on the surface of reused catalyst not only affect the reaction between active sites and fresh BPA solution, but also compete the reactive oxidant species in the subsequence reaction, leading to the declined removal efficiency. The XPS spectra also showed that the molar proportions of Co(III)/Co(II) were also reduced from 0.59 to 0.41 after the LCO/PMS reaction, while the proportions of OVs were slightly decreased. In addition, the mineralization extent of BPA was also explored by a TOC analyser. After 25 min of reaction, the TOC removal efficiency of BPA was 46.8% in the LCO/PMS processes. Moreover, the cobalt leaching was investigated by ICP measurement after the

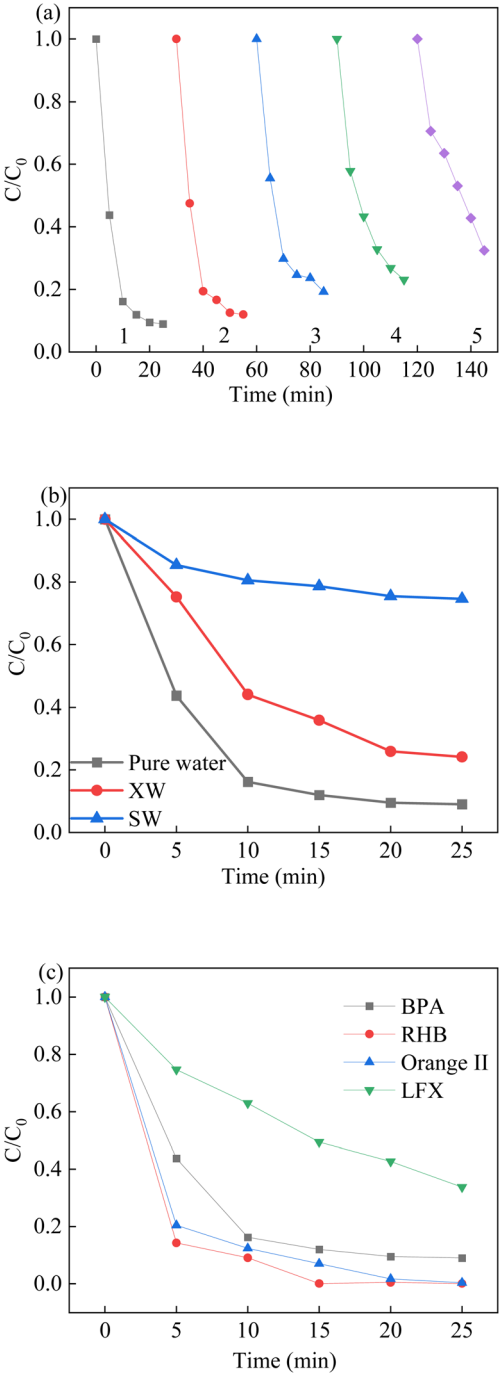

Fig. 11 (a) Reusability of LCO on BPA degradation, (b) effect of water matrix on BPA degradation, (c) different contaminants in the LCO/PMS systems. Reaction conditions: [BPA] = 0.05 mM, [PMS] = 1.0 mM, [LCO] = 0.5 g L^{-1}, initial PH = 6.8.

reaction. It was observed that 0.026 mg L^{-1} cobalt leached into the solution, indicating the good stability of the as-synthesized LCO. In order to prove the mechanism of heterogeneous catalyst activation of PMS, a homogeneous process was performed with leaching solution after the 25 min reaction. The removal of BPA was approximately 12.5%, which indicated that the catalytic activity was ascribed mainly to the heterogeneous LCO/PMS system.

The catalytic activity of the $La_2CoO_{4+\delta}$ materials for the other types of organic pollutants is also important and has a great influence on their practical usage in environmental remediation applications. Hence, the catalytic activity of $La_2CoO_{4+\delta}$ was determined for PMS activation with organic pollutants, such as Rhodamine B (RhB), Orange II (AO7) and Levofloxacin (LFX), which shown in Fig. 11c. The removal efficiencies of RhB, AO7 and LFX after 25 min were 100%, 100% and 66.3%, respectively. The results showed that the LCO/PMS system could efficiently degrade other types of organic pollutants, especially for the dye removal. In addition, different water matrixes were also used in this study to explore the applicability of LCO/PMS in real wastewater treatment. The degradation efficiency of BPA was 70.8% in XW water but decreased markedly in SW water, in which the co-existing anions have a negative effect on the BPA removal. In conclusion, the perovskite LCO was an efficient and stable catalyst for the PMS activation and the subsequent experiments.

4. Conclusions

In this study, $La_2CoO_{4+\delta}$ was successfully synthesized for the activation of PMS in BPA degradation with highly efficient catalytic activity. At a PMS concentration of 1.0 mM and catalyst dosage of 0.5 g L^{-1}, 91.1% removal of BPA was achieved. In the PMS activation process, certain reactive species were generated, leading to a high removal efficiency of BPA. Finally, the TOC results showed that the LCO/PMS system also presented a high mineralization rate. Quenching experiments showed that sulfate radicals played a dominant role during the activation of PMS. The LCO catalyst showed good stability and reusability during the reaction, exhibiting that LCO is a potential catalyst for good application to activate PMS for BPA degradation.

Author contributions

Methodology, X. Zhong; investigation, W. T. Wu, H. N. Jie and X. Zhong; resources, X. Zhong and F. B. Jiang; writing – original draft preparation, X. Zhong; writing – review and editing, X. Zhong; project administration, X. Zhong and F. B. Jiang.

Conflicts of interest

There are no conflicts to declare.

Acknowledgements

This work is financially supported by the Project of Innovative Foundation of Guangdong Province of China (Grant No. 2022KTSCX206), Project of Innovative Foundation of Guangdong Province of China (Grant No. 2020KTSCX177), Promotion Project Funds of Beijing Normal University, Zhuhai (Grant No. 201850001), Quality Engineering Project of Beijing Normal University, Zhuhai (Grant No. 201832) and Plan of Youth Teachers of Guangdong Higher Education Association (Grant No. 19GYB060). This work is financially supported by the Project of Youth Innovative Foundation of Guangdong Province

of China, Science Promotion Project Funds of Beijing Normal University, Zhuhai, Quality Engineering Project of Beijing Normal University, Zhuhai and Plan of Youth Teachers of Guangdong Higher Education Association for help in XRD, SEM, TEM and XPS analysis. AJE company was employed to edit for proper English language, grammar, punctuation, spelling, and overall style by one or more of the highly qualified native English-speaking editors.

References

1 L. Huang, X. Huang, J. Yan, Y. Liu, H. Jiang, H. Zhang, J. Tang and Q. Liu, Research progresses on the application of perovskite in adsorption and photocatalytic removal of water pollutants, *J. Hazard. Mater.*, 2023, **442**, 130024.

2 D. Ewis, M. M. Ba-Abbad, A. Benamor and M. H. El-Naas, Adsorption of organic water pollutants by clays and clay minerals composites: A comprehensive review, *Appl. Clay Sci.*, 2022, **229**, 106686.

3 C. Shi, X. Wang, S. Zhou, X. Zuo and C. Wang, Mechanism, application, influencing factors and environmental benefit assessment of steel slag in removing pollutants from water: A review, *J. Water Process. Eng.*, 2022, **47**, 102666.

4 W. Wang, H. Zhang, Y. Chen and H. Shi, Efficient Degradation of Tetracycline via Coupling of Photocatalysis and Photo-Fenton Processes over a 2D/2D α-Fe_2O_3/g-C_3N_4 S-Scheme Heterojunction Catalyst, *Acta Phys.-Chim. Sin.*, 2022, **38**, 2201008.

5 M. Kumar, S. Sridharan, A. D. Sawarkar, A. Shakeel, P. Anerao, G. Mannina, P. Sharma and A. Pandey, Current research trends on emerging contaminants pharmaceutical and personal care products (PPCPs): A comprehensive review, *Sci. Total Environ.*, 2023, **859**, 160031.

6 Y. Luo, G. Huang, Y. Li, Y. Yao, J. Huang, P. Zhang, S. Ren, J. Shen and Z. Zhang, Removal of pharmaceutical and personal care products (PPCPs) by MOF-derived carbons: A review, *Sci. Total Environ.*, 2023, **857**, 159279.

7 E. Couto, P. P. Assemany, G. C. A. Carneiro and D. C. F. Soares, The potential of algae and aquatic macrophytes in the pharmaceutical and personal care products (PPCPs) environmental removal: a review, *Chemosphere*, 2022, **302**, 134808.

8 O. Banerjee, S. Singh, I. Saha, S. Pal, M. Banerjee, S. Kundu, A. K. Syamal, B. K. Maji and S. Mukherjee, Molecular dissection of cellular response of pancreatic islet cells to Bisphenol-A (BPA): A comprehensive review, *Biochem. Pharmacol.*, 2022, **201**, 115068.

9 X. Fu, R. Yang, G. Zhou, X. Chen, Y. Liu, J. Chi, X. Li, H. Fang, H. Li and W. Li, New progress in photocatalytic degradation of bisphenol A as representative endocrine disrupting chemicals, *Curr. Opin. Green Sustainable Chem.*, 2022, **35**, 100629.

10 C. Xiao, L. Wang, Q. Zhou and X. Huang, Hazards of bisphenol A (BPA) exposure: A systematic review of plant toxicology studies, *J. Hazard. Mater.*, 2020, **384**, 121488.

11 Y. Hu, Q. Zhu, X. Yan, C. Liao and G. Jiang, Occurrence, fate and risk assessment of BPA and its substituents in wastewater treatment plant: A review, *Environ. Res.*, 2019, **178**, 108732.

12 J. L. Torres-García, M. Ahuactzin-Pérez, F. J. Fernández and D. V. Cortés-Espinosa, Bisphenol A in the environment and recent advances in biodegradation by fungi, *Chemosphere*, 2022, **303**, 134940.

13 S. Li, Y. Wu, H. Zheng, H. Li, Y. Zheng, J. Nan, J. Ma, D. Nagarajan and J. S. Chang, Antibiotics degradation by advanced oxidation process (AOPs): Recent advances in ecotoxicity and antibiotic-resistance genes induction of degradation products, *Chemosphere*, 2023, **311**, 136977.

14 Z. Honarmandrad, X. Sun, Z. Wang, M. Naushad and G. Boczkaj, Activated persulfate and peroxymonosulfate based advanced oxidation processes (AOPs) for antibiotics degradation-A review, *Water Resour. Ind.*, 2022, 100194.

15 C. Dong, W. Fang, Q. Yi and J. Zhang, A comprehensive review on reactive oxygen species (ROS) in advanced oxidation processes (AOPs), *Chemosphere*, 2022, **308**, 136205.

16 W. Lin, X. Liu, A. Ding, H. H. Ngo, R. Zhang, J. Nan, J. Ma and G. Li, Advanced oxidation processes (AOPs)-based sludge conditioning for enhanced sludge dewatering and micropollutants removal: A critical review, *J. Water Process. Eng.*, 2022, **45**, 102468.

17 M. P. Rayaroth, C. T. Aravindakumar, N. S. Shah and G. Boczkaj, Advanced oxidation processes (AOPs) based wastewater treatment-unexpected nitration side reactions-a serious environmental issue: A review, *Chem. Eng. J.*, 2022, **430**, 133002.

18 P. Yuan, H. Ma, B. Shen and Z. Ji, Abatement of NO/SO_2/Hg^0 from flue gas by advanced oxidation processes (AOPs): Tech-category, status quo and prospects, *Sci. Total Environ.*, 2022, **806**, 150958.

19 G. AdisuryaIsmail and H. Sakai, Review on effect of different type of dyes on advanced oxidation processes (AOPs) for textile color removal, *Chemosphere*, 2022, **291**, 132906.

20 J. Xie, C. Zhang and T. D. Waite, Hydroxyl radicals in anodic oxidation systems: generation, identification and quantification, *Water Res.*, 2022, **217**, 118425.

21 G. Wang, Y. Iradukunda, G. Shi, P. Sanga, X. Niu and Z. Wu, Hydroxyl, hydroperoxyl free radicals determination methods in atmosphere and troposphere, *J. Environ. Sci.*, 2021, **99**, 324–335.

22 Y. Liu, Y. Zhao and J. Wang, Fenton/Fenton-like processes with in-situ production of hydrogen peroxide/hydroxyl radical for degradation of emerging contaminants: Advances and prospects, *J. Hazard. Mater.*, 2021, **404**, 124191.

23 P. V. Nidheesh, G. Divyapriya, F. E. Titchou and M. Hamdani, Treatment of textile wastewater by sulfate radical based advanced oxidation processes, *Sep. Purif. Technol.*, 2022, **293**, 121115.

24 Z. Gao, J. Zhu, Q. Zhu, C. Wang and Y. Cao, Spinel ferrites materials for sulfate radical-based advanced oxidation process: A review, *Sci. Total Environ.*, 2022, **847**, 157405.

25 E. Domingues, M. J. Silva, T. Vaz, J. Gomes and R. C. Martins, Sulfate radical based advanced oxidation processes for agro-

industrial effluents treatment: A comparative review with Fenton's peroxidation, *Sci. Total Environ.*, 2022, **832**, 155029.
26 X. Duan, X. Niu, J. Gao, S. Wacławek, L. Tang and D. D. Dionysiou, Comparison of sulfate radical with other reactive species, *Curr. Opin. Chem. Eng.*, 2022, **38**, 100867.
27 A. Yusuf, A. Giwa, J. O. Eniola, H. K. Amusa and M. R. Bilad, Recent advances in catalytic sulfate radical-based approach for removal of emerging contaminants, *J. Hazard. Mater. Adv.*, 2022, **7**, 100108.
28 X. Li, B. Jie, H. Lin, Z. Deng, J. Qian, Y. Yang and X. Zhang, Application of sulfate radicals-based advanced oxidation technology in degradation of trace organic contaminants (TrOCs): Recent advances and prospects, *J. Environ. Manage.*, 2022, **308**, 114664.
29 H. Chen, Y. Xu, K. Zhu and H. Zhang, Understanding oxygen-deficient $La_2CuO_{4-\delta}$ perovskite activated peroxymonosulfate for bisphenol A degradation: The role of localized electron within oxygen vacancy, *Appl. Catal., B*, 2021, **284**, 119732.
30 A. Margellou, D. Manos, D. Petrakis and I. Konstantinou, Activation of persulfate by $LaFe_{1-x}Co_xO_3$ perovskite catalysts for the degradation of phenolics: Effect of synthetic method and metal substitution, *Sci. Total Environ.*, 2022, **832**, 155063.
31 S. Wang, Y. Zhang, S. Zhao, Y. Zhang, Y. Wang, Y. Zhang, A. Kang, E. Duan and S. Qiao, A facile approach to improve the methane catalytic performance of $LaCoO_3$ perovskite, *Mol. Catal.*, 2022, **531**, 112685.
32 N. K. Labhsetwar, A. Watanabe and T. Mitsuhashi, New improved syntheses of $LaRuO_3$ perovskites and their applications in environmental catalysis, *Appl. Catal., B*, 2003, **40**(1), 21–30.
33 F. Mahmoudi, K. Saravanakumar, V. Maheskumar, L. K. Njaramba, Y. Yoon and C. M. Park, Application of perovskite oxides and their composites for degrading organic pollutants from wastewater using advanced oxidation processes: Review of the recent progress, *J. Hazard. Mater.*, 2022, **436**, 129074.
34 K. Wei, Y. Faraj, G. Yao, R. Xie and B. Lai, Strategies for improving perovskite photocatalysts reactivity for organic pollutants degradation: A review on recent progress, *Chem. Eng. J.*, 2021, **414**, 128783.
35 D. Y. Heo, W. J. Jang and S. Y. Kim, Recent review of interfacial engineering for perovskite solar cells: effect of functional groups on the stability and efficiency, *Mater. Today Chem.*, 2022, **26**, 101224.
36 C. Chen, R. Bao, L. Yang, S. Tai, Y. Zhao, W. Wang, J. Xia and H. Li, Application of inorganic perovskite $LaNiO_3$ partial substituted by Ce and Cu in absorbance and photocatalytic degradation of antibiotics, *Appl. Surf. Sci.*, 2022, **579**, 152026.
37 H. Peng, W. Zhang, Y. Song, F. Yin, C. Zhang and L. Zhang, In situ construction of Co/Co_3O_4 with N-doped porous carbon as a bifunctional electrocatalyst for oxygen reduction and oxygen evolution reactions, *Catal. Today*, 2020, **355**, 286–294.
38 E. V. Dokuchits, T. V. Larina, A. V. Ishchenko and T. P. Minyukova, The effect of substituting La and Co with Ca and Ti in $LaCoO_3$/KIT-6 on its properties and possible catalytic application in syngas conversion, *Mater. Chem. Phys.*, 2022, **276**, 125387.
39 T. Waki, S. Okazaki, Y. Tabata, M. Kato, K. Hirota and H. Nakamura, Effect of oxygen potential on Co solubility limit in La–Co co-substituted magnetoplumbite-type strontium ferrite, *Mater. Res. Bull.*, 2018, **104**, 87–91.
40 S. Podila, H. Driss, A. M. Ali, A. A. Al-Zahrani and M. A. Daous, Influence of Ce substitution in $LaMO_3$ (M = Co/Ni) perovskites for CO_x-free hydrogen production from ammonia decomposition, *Arabian J. Chem.*, 2022, **15**(1), 103547.
41 J. G. Bednorz, M. Takashige and K. A. Müller, Preparation and characterization of alkaline-earth substituted superconducting La_2CuO_4, *Mater. Res. Bull.*, 1987, **22**(6), 819–827.
42 Y. Yulizar, D. O. B. Apriandanu and R. I. Ashna, La_2CuO_4-decorated ZnO nanoparticles with improved photocatalytic activity for malachite green degradation, *Chem. Phys. Lett.*, 2020, **755**, 137749.
43 L. D. Santos-Gómeza, J. M. Porras-Vázquez, J. Hurtado, E. R. Losilla and D. Marrero-López, Stability and electrochemical performance of nanostructured $La_2CuO_{4+\delta}$ cathodes, *J. Alloys Compd.*, 2019, **788**, 565–572.
44 M. Hammad, B. Alkan, A. K. Al-kamal, C. Kim, M. Y. Ali, S. Angel, H. T. A. Wiedemann, D. Klippert, T. C. Schmidt, C. W. M. Kay and H. Wiggers, Enhanced heterogeneous activation of peroxymonosulfate by Ruddlesden-Popper-type $La_2CoO_{4+\delta}$ nanoparticles for bisphenol A degradation, *Chem. Eng. J.*, 2022, **429**, 131447.
45 T. Ghorbani-Moghadam, H. A. R. Aliabad and M. Mousavi, Optoelectronic properties of La_2CoO_4 and $LaSrCoO_4$ Ruddlesden-Popper compounds: Comparative experimental and DFT studies by GGA/MBJ + U, *Mater. Sci. Eng., B*, 2022, **286**, 116074.
46 Y. Li, Y. Wang, L. Liu and L. Tian, Oxygen-vacancy abundant electrospun Co-doped Ruddlesden-Popper perovskite catalysts for peroxymonosulfate activation and Rhodamine B degradation, *J. Cleaner Prod.*, 2022, **380**, 135117.
47 P. Liang, D. Meng, Y. Liang, Z. Wang, C. Zhang, S. Wang and Z. Zhang, Cation deficiency tuned $LaCoO_{3-\delta}$ perovskite for peroxymonosulfate activation towards bisphenol A degradation, *Chem. Eng. J.*, 2021, **409**, 128196.
48 H. Guo, X. Zhou, Y. Zhang, Q. Yao, Y. Qian, H. Chu and J. Chen, Carbamazepine degradation by heterogeneous activation of peroxymonosulfate with lanthanum cobaltite perovskite: Performance, mechanism and toxicity, *J. Environ. Sci.*, 2020, **91**, 10–21.
49 X. Bu, C. Chen, X. Zhao, Q. Huang, X. Liao, H. Fan, P. Wang, H. Hu, Y. Zhang and Z. Huang, Fabrication of novel Z-scheme $LaCoO_3$/activated biochar/Ag_3PO_4 heterojunctions for intensifying visible-light-catalytic degradation of bisphenol A, *Appl. Surf. Sci.*, 2022, **588**, 152887.
50 R. Zhang, Y. Wan, J. Peng, G. Yao, Y. Zhang and B. Lai, Efficient degradation of atrazine by $LaCoO_3/Al_2O_3$ catalyzed peroxymonosulfate: Performance, degradation

intermediates and mechanism, *Chem. Eng. J.*, 2019, **372**, 796–808.

51 X. Pang, Y. Guo, Y. Zhang, B. Xu and F. Qi, $LaCoO_3$ perovskite oxide activation of peroxymonosulfate for aqueous 2-phenyl-5-sulfobenzimidazole degradation: Effect of synthetic method and the reaction mechanism, *Chem. Eng. J.*, 2016, **304**, 897–907.

52 C. Feng, Q. Gao, G. Xiong, Y. Chen, Y. Pan, Z. Fei, Y. Li, Y. Lu, C. Liu and Y. Liu, Defect engineering technique for the fabrication of $LaCoO_3$ perovskite catalyst via urea treatment for total oxidation of propane, *Appl. Catal., B*, 2022, **304**, 121005.

53 Q. Pan, Q. Gao, G. Gao, M. Liu, B. Han, K. Xia and C. Zhou, Composition-engineered $LaCoO_3$-based monolithic catalysts for easily operational and robust peroxymonosulfate activation, *Chem. Eng. J.*, 2021, **424**, 130574.

54 D. Kiejza, U. Kotowska, W. Polińska and J. Karpińska, Peracids - New oxidants in advanced oxidation processes: The use of peracetic acid, peroxymonosulfate, and persulfate salts in the removal of organic micropollutants of emerging concern-A review, *Sci. Total Environ.*, 2021, **790**, 148195.

55 X. Duan, C. Su, J. Miao, Y. Zhong, Z. Shao, S. Wang and H. Sun, Insights into perovskite-catalyzed peroxymonosulfate activation: Maneuverable cobalt sites for promoted evolution of sulfate radicals, *Appl. Catal., B*, 2018, **220**, 626–634.

56 A. Hassani, J. Scaria, F. Ghanbari and P. V. Nidheesh, Sulfate radicals-based advanced oxidation processes for the degradation of pharmaceuticals and personal care products: A review on relevant activation mechanisms, performance, and perspectives, *Environ. Res.*, 2022, 114789.

57 S. Li, Y. Wu, Y. Zheng, J. Ma, H. Zheng and S. You, Black phosphorus quantum dots regulate electronic structure of perovskite catalyst for enhanced peroxodisulfate activation and non-radical decontamination, *Appl. Catal., B*, 2022, **319**, 121930.

58 L. Yang, Y. Jiao, D. Jia, Y. Li and C. Liao, Role of oxygen vacancies and Sr sites in $SrCo_{0.8}Fe_{0.2}O_3$ perovskite on efficient activation of peroxymonosulfate towards the degradation of aqueous organic pollutants, *Chin. J. Chem. Eng.*, 2021, **40**, 269–277.

59 J. Hou, X. He, S. Zhang, J. Yu, M. Feng and X. Li, Recent advances in cobalt-activated sulfate radical-based advanced oxidation processes for water remediation: A review, *Sci. Total Environ.*, 2021, **770**, 145311.

60 Y. Wu, Y. Xing, X. Zhao, Z. Zhou and G. Jing, Mechanistic insights into rapid sulfite activation with cobalt sulfide towards iohexol abatement: Contribution of sulfur conversion, *Chem. Eng. J.*, 2022, **429**, 132404.

61 J. Tan, J. Wang, Z. Tan, M. Yu, Z. Yang, Z. Ren, Y. Li, Y. Zhang and X. Lin, Efficient activation of peroxydisulfate by a novel magnetic nanocomposite lignin hydrogel for contaminant degradation: Radical and nonradical pathways, *Chem. Eng. J.*, 2023, **451**, 138504.

62 X. Zhao, J. Jiang, S. Pang, C. Guan, J. Li, Z. Wang, J. Ma and C. Luo, Degradation of iopamidol by three UV-based oxidation processes: Kinetics, pathways, and formation of iodinated disinfection byproducts, *Chemosphere*, 2019, **221**, 270–277.

63 L. Zhang, N. Yang, Y. Han, X. Wang, S. Liu, L. Zhang, Y. Sun and B. Jiang, Development of polyacrylonitrile/perovskite catalytic membrane with abundant channel-assisted reaction sites for organic pollutant removal, *Chem. Eng. J.*, 2022, **437**, 135163.

64 S. Wu, Y. Lin, C. Yang, C. Du, Q. Teng, Y. Ma, D. Zhang, L. Nie and Y. Zhong, Enhanced activation of peroxymonosulfte by $LaFeO_3$ perovskite supported on Al_2O_3 for degradation of organic pollutants, *Chemosphere*, 2019, **237**, 124478.

65 J. Li, W. Ma, D. Zhong, K. Li, J. Ma, S. Zhang and X. Du, Oxygen vacancy concentration modulation of perovskite-based heterogeneous catalysts for Fenton-like oxidation of tetracycline, *J. Cleaner Prod.*, 2022, **362**, 132469.

66 C. Su, R. Li, C. Li and W. Wang, Piezo-promoted regeneration of Fe^{2+} boosts peroxydisulfate activation by $Bi_2Fe_4O_9$ nanosheets, *Appl. Catal., B*, 2022, **310**, 121330.

67 N. P. Ferraz, A. E. Nogueira, F. C. F. Marcos, V. A. Machado, R. R. Rocca, E. M. Assaf and Y. J. O. Asencios, CeO_2–Nb_2O_5 photocatalysts for degradation of organic pollutants in water, *Rare Met.*, 2020, **39**, 230–240.

68 R. R. Solis, F. J. Rivas and O. Gimeno, Removal of aqueous metazachlor, tembotrione, tritosulfuron and ethofumesate by heterogeneous monopersulfate decomposition on lanthanum-cobalt perovskites, *Appl. Catal., B*, 2017, **200**, 83–92.

69 K. Y. A. Lin, Y. C. Chen, T. Y. Lin and H. Yang, Lanthanum cobaltite perovskite supported on zirconia as an efficient heterogeneous catalyst for activating Oxone in water, *J. Colloid Interface Sci.*, 2017, **497**, 325–332.